CHEMISTRY OF MATERIALS

pubs.acs.org/cm

Article

Smart Microcapsules Designed for On-Demand Local Heating and Drug Release

Ji-Won Kim,[⊥] Sang Hoon Han,[⊥] Minhee Ku,[⊥] Jaemoon Yang,* and Shin-Hyun Kim*

Cite This: https://doi.org/10.1021/acs.chemmater.3c00517

Read Online

ACCESS | Metrics & More | Article Recommendations | Supporting Information

ABSTRACT: Chemophotothermal therapy is promising for cancer treatment with its synergistic effect. Although various photothermal agents have been formulated as drug carriers, low payload, burst release, and severe dilution usually restrict their uses. To overcome the limitations, we design smart microcapsules as a pragmatic material for chemophotothermal therapy. With a microfluidic device, water-in-oil-in-water (W/O/W) double-emulsion templates are produced to have photothermal polydopamine nanoparticles and drugs in the water core and a mixture of photocurable monomers and phase-change material (PCM) in the oil shell. The droplets are significantly shrunken by the osmotic extraction of water from the core, which enables the size reduction for the ease of injection and enrichment of polydopamine nanoparticles and drugs for enhanced photothermal performance and high payload. The microcapsules, produced by photopolymerization of monomers, release drugs when PCM in continuous nanochannels of the polymer shell is molten while retaining drugs without leakage when frozen. As the concentrated polydopamine nanoparticles provide rapid and drastic heating by near-infrared irradiation, the drug release can be switched on and off in a programmed manner by manipulating the irradiation. The smart microcapsules secure high drug payload in a spacious core, negligible initial bursting, and dilution-free high photothermal performance, potentially serving as a pragmatic therapy platform.

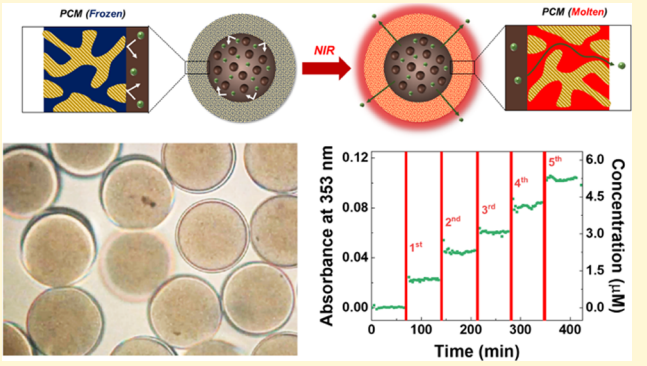

1. INTRODUCTION

Photothermal therapy treats cancers by elevating the temperature through the conversion of radiation energy to heat. Therefore, the therapy is noninvasive and highly localized, which can reduce the potential side effects of chemotherapy and surgery.[1] Various photothermal agents have been employed for the efficient conversion of near-infrared (NIR) to heat as NIR has a relatively long penetration depth along the skin and tissue. For example, gold nanorods,[2−7] carbon nanotubes,[8] reduced graphene oxide,[9−13] and graphene quantum dots[14−16] have been synthesized and intensively used for photothermal heating under NIR irradiation. Biocompatible organic materials, such as polydopamine,[17−22] polyaniline,[23−28] and polypyrrole,[29−32] also have been used as excellent photothermal agents, which are advantageous as tissue-injury-causing oxidative stress can be alleviated. It is of great importance to design photothermal agents for rapid heating at a specific localized region to minimize the side effects after thermal ablation.

Recently, chemophotothermal therapy is emerging as an advanced method for cancer treatment as it provides a synergistic effect.[33] To release anticancer drugs into the locally heated tumor, the photothermal agents have been hybridized into drug carriers.[34] For example, multilayered nanosheets of reduced graphene oxide are used to physically adsorb doxorubicin in the interstitial voids and release the drug under NIR irradiation.[35] Mesoporous silica nanoparticles are also used to entrap doxorubicin in the pores, which are closed with graphene quantum dots[36] or polydopamine coating.[37] However, most of the chemophotothermal agents have low payload and poor encapsulation efficiency. Furthermore, the anticancer drugs usually are leaked out from the agents without NIR irradiation as they are physically adsorbed or loosely trapped, restricting long-term storage. More importantly, the drugs are burst-released upon NIR irradiation, lowering the efficacy of the drugs and causing severe side effects. Therefore, microcarriers that provide the stable storage and controlled release of anticancer drugs, as well as high payload and encapsulation efficiency, are highly demanding for synergistic chemophotothermal therapy.

Herein, we report NIR-responsive microcapsules as a novel and pragmatic chemophotothermal platform. The micro-

Received: March 6, 2023
Revised: May 23, 2023

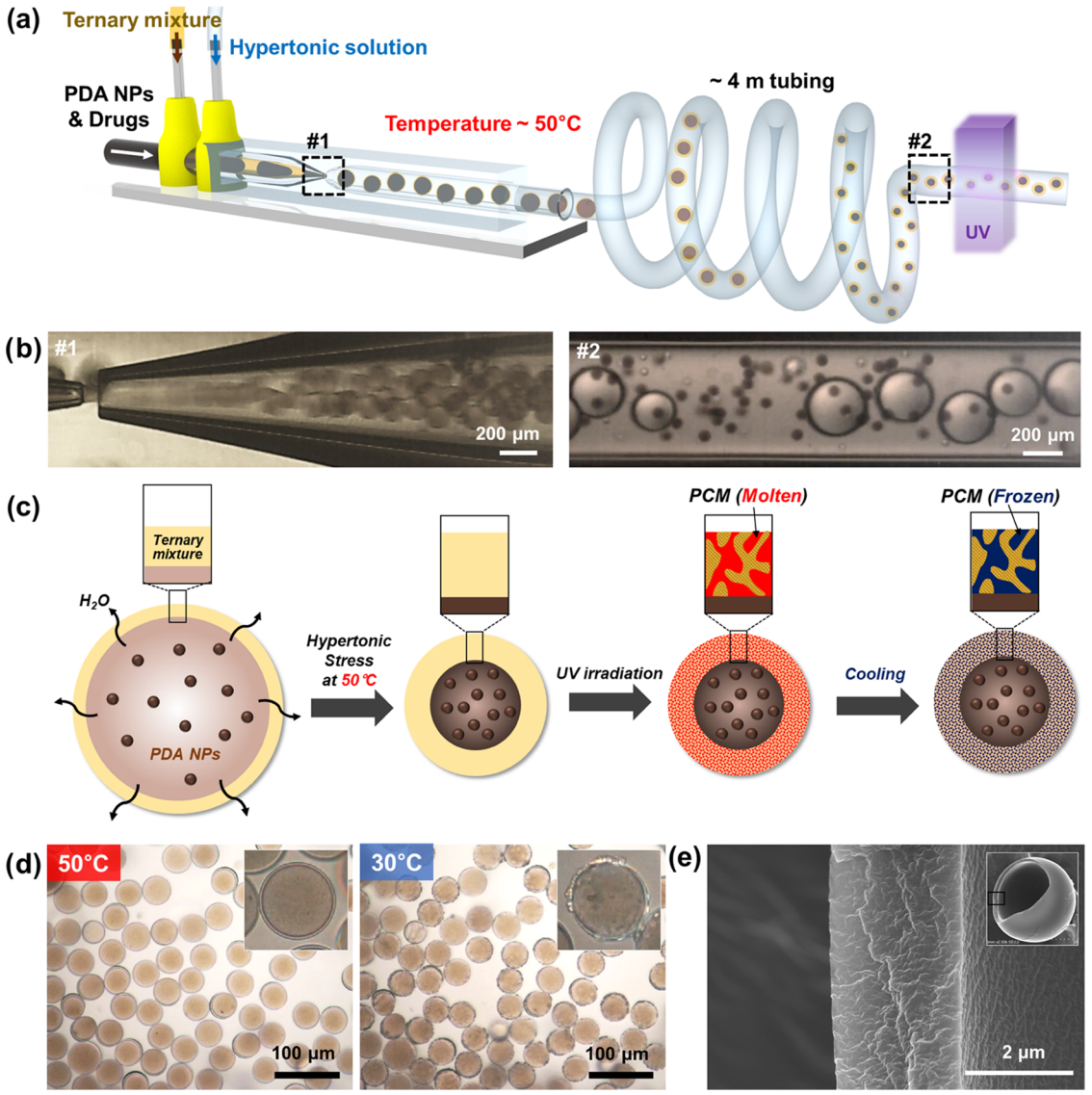

Figure 1. (a) Schematic for a capillary microfluidic device for producing ultrathin-shelled water-in-oil-in-water (W/O/W) double-emulsion droplets and osmotically extracting water from the innermost droplets. (b) Stillshot images showing the generation of double-emulsion droplets at the junction (#1) and the flow of shrunken droplets downstream (#2). (c) Cartoons showing three steps for the production of microcapsules: osmotic extraction of water for the enrichment of encapsulants, UV irradiation for photopolymerization in the shell, and cooling to room temperature for freezing phase-change material (PCM) in the shell. (d) Optical microscope (OM) images showing the polymerized microcapsules at 50 °C (the left panel) and 30 °C (the right panel). The insets are magnified views. (e) Scanning electron microscope (SEM) image showing the cross section of the shell of the microcapsule. The inset is a low-magnification image of the microcapsule.

capsules contain highly concentrated polydopamine (PDA) nanoparticles and anticancer drugs in their spacious aqueous core, enclosed by a thin thermoresponsive shell. The shell membrane consists of phase-change material (PCM) nanochannels in a polymeric framework, which selectively allows the release of the drugs in a sustained manner above the melting point of the PCM. The PDA nanoparticles in the core show a strong photothermal effect so that the microcapsules are locally heated under NIR irradiation at which the drugs are released. The microcapsules are small enough to be injected through a needle but large enough to be implanted into target tumor sites without diffusion. To produce the chemo-photothermal microcapsules, we use water-in-oil-in-water (W/O/W) double-emulsion templates. With a capillary microfluidic device, double-emulsion droplets are produced to have the inner water drop containing PDA nanoparticles and drugs and the outer oil drop of photocurable monomer, PCM, and molecular compatibilizer. To concentrate the PDA nanoparticles and drugs in the core and reduce the size of microcapsules, the double-emulsion drops are subjected to a strong hypertonic condition in the device, which are then stabilized by *in situ* photopolymerization of monomer. This microfluidic approach provides a high payload and high encapsulation efficiency. The microcapsules show a negligible leakage of drugs during storage at low temperatures, which provide rapid local heating upon the irradiation of an 808 nm laser and a gradual release of the drugs. The release is held up when the laser is off as the temperature drops quickly because the heating is highly localized. Therefore, the drug can be released in a programmed fashion by controlling laser irradiation. We believe that our microcapsule platform is

https://doi.org/10.1021/acs.chemmater.3c00517
Chem. Mater. XXXX, XXX, XXX−XXX

highly valuable as a novel and pragmatic chemophotothermal agent for efficient cancer treatment.

2. RESULTS AND DISCUSSION

2.1. Microfluidic Production of NIR-Responsive Microcapsules. The microcapsules for chemophotothermal therapy should provide photothermal heating and drug release at local regions under NIR irradiation. To achieve this function, we design microcapsules composed of a PDA nanoparticle-laden aqueous core and a PCM−polymer composite shell. The PDA nanoparticles serve as an efficient photothermal agent so that the temperature can be increased upon NIR irradiation. The composite shell consists of interconnected PCM nanochannels in a polymeric matrix, which selectively allows the transmembrane transport of molecules that are soluble in molten PCM at temperatures above the melting point. Therefore, photothermal heating can trigger the release of anticancer drugs as long as the temperature is increased above the melting point and drugs are soluble in the molten PCM. To produce microcapsules with such a construction, we use a W/O/W double-emulsion template. The template is produced in a uniform size by using capillary microfluidic devices. To maximize the core volume for drug loading and minimize the diffusion length for release, thin shells are prepared. We use the design of the capillary devices for the production of double-emulsion drops with an ultrathin shell that employs the emulsification of core−sheath flow at the junction between two tapered capillaries with a tip-to-tip alignment, as illustrated in Figure 1a.[38−40]

As the innermost phase, an aqueous dispersion of 0.17 w/w % melanin-coated PDA nanoparticles with an average diameter of 100 nm containing 5 w/w% poly(vinyl alcohol) (PVA) is used; the solution has an osmolarity of 40 mOsmol/L, and the melanin-coated PDA nanoparticles are shown in Figure S1. To compose the PCM−polymer composite shell, we use a homogeneous mixture of 29 w/w% of 1-tetradecanol, 35 w/w% of trimethylolpropane ethoxylate triacrylate (ETPTA), 35 w/w% of lauryl acrylate (LA), and 1 w/w% of photoinitiator as the middle oil phase. As PCM, 1-tetradecanol is selected because its melting point, T_m = 38 °C, is slightly higher than the body temperature. That is, the PCM will remain frozen when injected into a body so that the undesired release in the absence of photothermal heating can be minimized. ETPTA forms a polymeric matrix through photo-cross-linking, whereas LA prevents a severe phase separation between the ETPTA and 1-tetradecanol as a molecular compatibilizer.[41] The innermost and middle phases are simultaneously injected into a cylindrical capillary with a hydrophobic inner wall. All phases are preheated to 50 °C, and the device is also operated at 50 °C to maintain the middle oil phase as a liquid. The innermost phase flows through the center of the capillary without contacting the hydrophobic wall, forming a train of plug-shaped drops, while the middle phase wets the wall and forms a continuous phase in the capillary. This discontinuous core−sheath flow is emulsified by a flow-focusing effect, at the tip of the capillary, into the continuous phase of the aqueous solution of 10 w/w% of PVA and 250 mM of NaCl, which is injected along the outer hydrophilic surface of the capillary. When the core−sheath flow of the plug-like drops is emulsified, monodisperse W/O/W double-emulsion droplets with an ultrathin shell are produced, as shown in the left panel of Figure 1b and Movie S1. When the oil phase flows out from the capillary, large oil drops are produced. Both small double-emulsion drops and large oil drops flow through the capillary on the opposite side and 4 m long tubing.

The double-emulsion drops produced at the junction have a typical size of 75 μm, which frequently causes the clogging of needles during the injection of polymerized microcapsules. Furthermore, it is required to increase the concentration of PDA nanoparticles in the core to enhance photothermal performance. However, it is challenging to increase the concentration of the melanin-coated PDA nanoparticles above 0.2 w/w% without aggregation using a conventional centrifugation method although melanin coating on PDA nanoparticles improves the dispersion stability, as shown in Figure S2. To reduce the size of microcapsules and increase the concentration of PDA nanoparticles at the same time, we use the continuous phase containing 250 mM NaCl with an osmolarity of 600 mOsmol/L to make a hypertonic condition. The osmotic-pressure difference between the innermost droplets and the continuous phase pumps water out, leading to the shrinkage of the double-emulsion drops, as illustrated in the left two panels of Figure 1c. The shrinkage is observed for the flowing drops downstream along the 4 m long tubing, as shown in the right panel of Figure 1b and Movie S1. With typical flow rates of the innermost, middle, and continuous phases of 350, 650, and 3500 μL/h, the double-emulsion drops with an average diameter of 75 μm are initially produced, which shrink to have an average diameter of 38 μm during the flow with a residence time of 0.44 h in the 4 m long tubing. The osmotic-pressure-induced water extraction leads to the enrichment in a factor of 7.7, resulting in a concentration of 1.3 w/w% of melanin-coated PDA nanoparticles. It is noteworthy that the double-emulsion drops rupture when they are incubated at the same hypertonic condition after collection. This is because the light innermost droplet migrates upward in the heavy oil shell, which eventually causes direct contact of the innermost droplet to the continuous phase, leading to internal coalescence. The double-emulsion drops tumble during the flow, which minimizes the off-centering of the innermost droplets, enabling the maintenance of the core−shell geometry.

The shrunken double-emulsion drops are continuously irradiated by ultraviolet (UV) at the exit of the tubing to copolymerize ETPTA and LA in the shell. The resulting microcapsules are highly uniform and contain a homogeneous dispersion of PDA nanoparticles in the core, as shown in the left panel of Figure 1d. The gentle osmotic enrichment does not cause severe aggregation. The large oil drops coproduced by the emulsification of discontinuous core−sheath flow form large particles, which are easily separated from the microcapsules by exploiting the density and size difference, as shown in Figure S3. For comparison, microcapsules are also produced without osmosis in an isotonic condition, which have an average diameter of 75 μm, as shown in Figure S4a. The solidified shell is composed of a polymeric matrix of ETPTA-LA at which 1-tetradecanol forms an interconnected channel network, as schematically illustrated in the third panel of Figure 1c. The PCM−polymer composite shell is highly homogeneous and transparent above the melting point of 1-tetradecanol.

When the microcapsules are cooled below the melting point, the shells turn to be heterogeneous and slightly opaque as the frozen 1-tetradecanol partially extrudes from the nanochannels, as shown in the right panel of Figure 1d. When the microcapsules are heated above the melting point, they recover

https://doi.org/10.1021/acs.chemmater.3c00517
Chem. Mater. XXXX, XXX, XXX−XXX

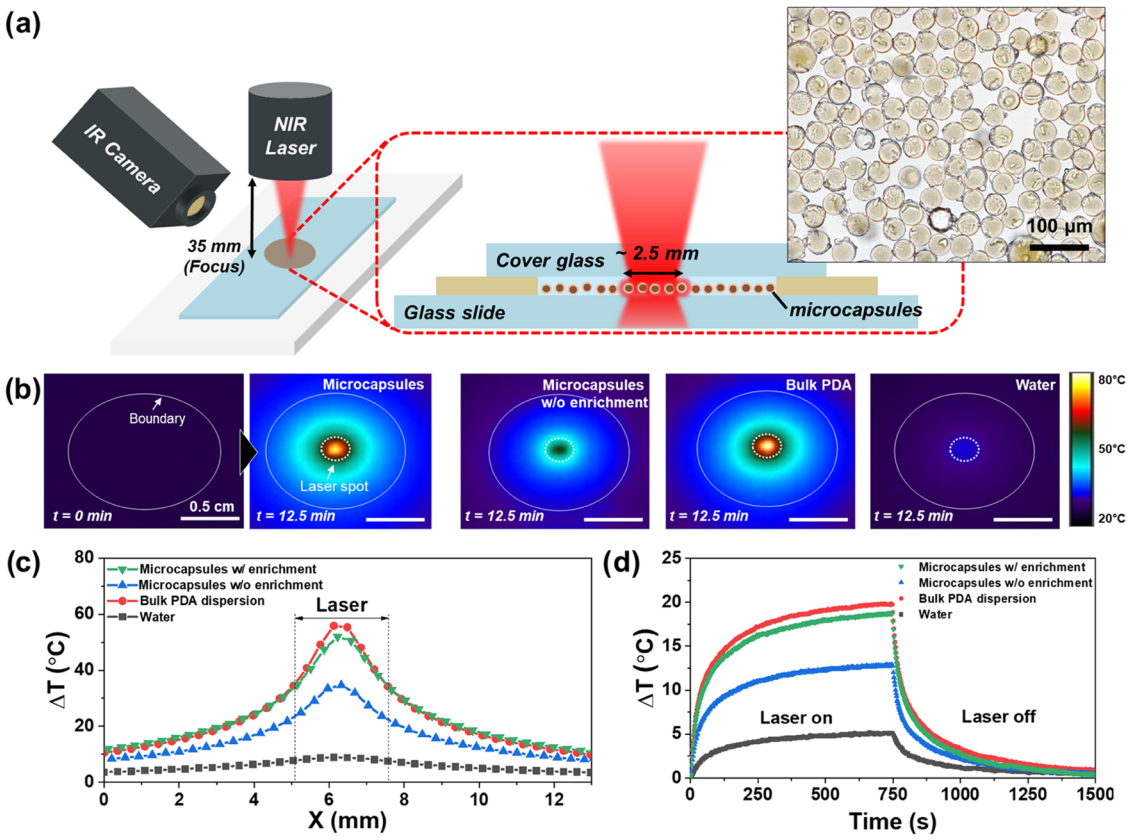

Figure 2. (a) Schematic for the experimental setup to study the photothermal effect. A monolayer of microcapsules in a chamber is irradiated by an 808 nm laser with a spot diameter of 2.5 mm, and the well is monitored with an infrared (IR) camera. The inset is an OM image of the microcapsules. (b) Temperature maps before laser irradiation (the leftmost), after laser irradiation for 12.5 min on the array of the microcapsules (the second), the array of microcapsules without enrichment (the third), bulk dispersion of polydopamine (PDA) nanoparticles (the fourth), and water (the rightmost). The boundaries of the laser spot and chamber are denoted. (c) Profiles of temperature increase from the initial for the four samples in panel (b) after laser irradiation for 12.5 min. (d) Temporal change of the temperature increase averaged for the entire volume of chamber for the four samples during laser-induced heating for 12.5 min and natural cooling for 12.5 min.

their original state. These two states are reversibly switchable by temperature swings as shown in Movie S2. It seems that the molten PCM fills the nanochannels above the melting point. The shells have an average thickness of 2.5 μm; the thickness of the original shell of the double-emulsion droplets before the shrinkage is estimated as 0.8 μm from the volume conservation. The removal of 1-tetradecanol by washing with isopropanol does not reveal any macroscopic channels or pores in the cross section of the shell, as shown in Figure 1e. It seems that 1-tetradecanol produces nanochannels in the presence of a molecular compatibilizer, LA, in the absence of macroscopic phase separation.[41]

2.2. Photothermal Heating with Microcapsules. PDA nanoparticles are one of the efficient photothermal agents, so it is expected that the microcapsules containing highly concentrated PDA nanoparticles show excellent performance in photothermal heating. To analyze the performance, a monolayer of the microcapsules with an average diameter of 38 μm in 5 w/w% of PVA solution is prepared in a 120 μm thick disk-shaped chamber with a diameter of 1.3 cm sandwiched by two glass slides, as shown in Figure 2a. The array of microcapsules is irradiated by a laser with a wavelength of 808 nm, a power of 650 mW, and a spot diameter of approximately 2.5 mm. The temporal change of temperature distribution is monitored with an infrared (IR) camera, as shown in Movie S3. The temperature increases over the irradiation time, where the highest temperature, T_h, is observed at the central position of the laser spot. For the irradiation of 12.5 min, the highest temperature at the center reaches as high as 78 °C, as shown in the second panel of Figure 2b; a local temperature around each microcapsule is expected to be much higher than T_h.

We compare the photothermal performance with the microcapsules with an average diameter of 75 μm prepared without osmotic-pressure-induced enrichment so that the concentration of PDA nanoparticles is 0.17 w/w% in the core, as shown in the third panel of Figure 2b; the monolayer of the microcapsules in the chamber is shown in Figure S5. The highest temperature increases up to 59 °C in 12.5 min. That is, the temperature increase is 67% of the microcapsules osmotically enriched. Considering that the total volume of microcapsules with a diameter of 75 μm in the monolayer is 2.0 times larger than those with a diameter of 38 μm, we can conclude that highly concentrated PDA nanoparticles of 1.3 w/w% are beneficial for photothermal heating. For bulk dispersion of PDA nanoparticles at a concentration of 0.17 w/w% without encapsulation, the temperature increases to 81 °C in 12.5 min, as shown in the fourth panel, which is comparable with the enriched microcapsules. Even though the enriched microcapsules occupy only 17% of the chamber volume, whereas the bulk dispersion fills out the entire volume, highly concentrated PDA nanoparticles in the core provide a high

https://doi.org/10.1021/acs.chemmater.3c00517
Chem. Mater. XXXX, XXX, XXX−XXX

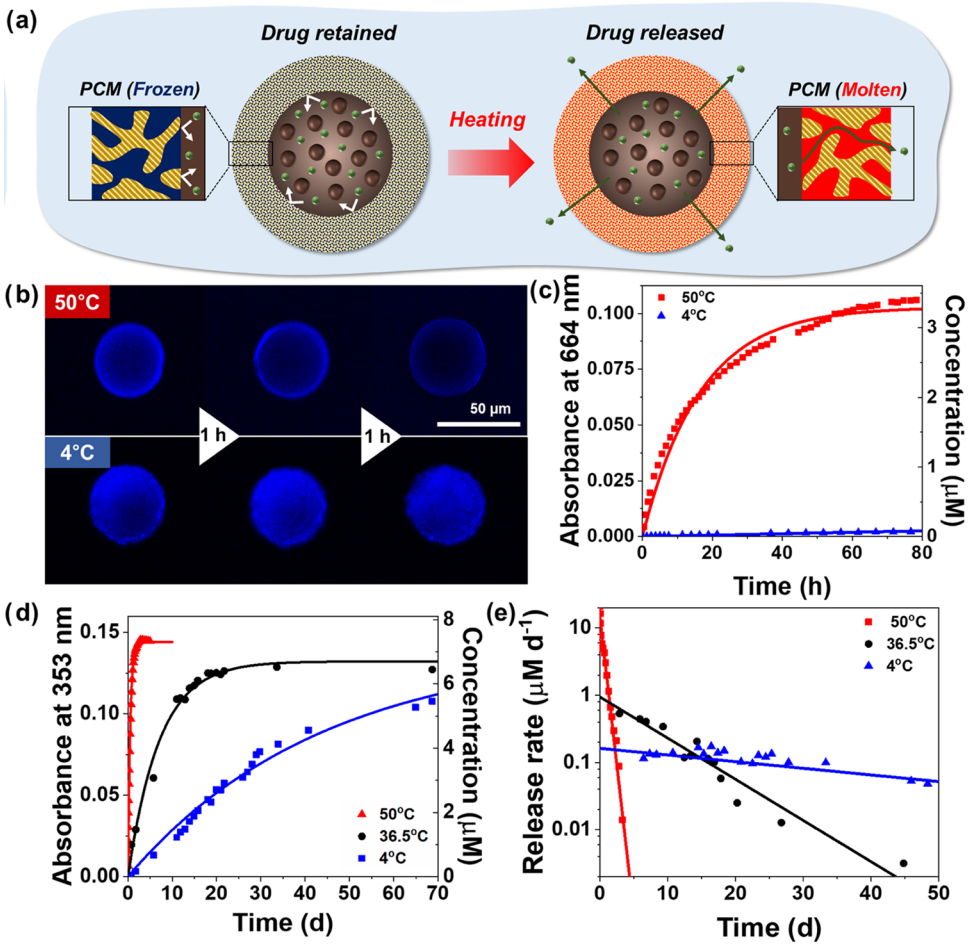

Figure 3. (a) Schematic for the temperature-responsive release of drug from the microcapsules. PCM is frozen in the nanochannel of the shell below its melting point, and no release is allowed, whereas it is molten above the melting point and the drug is released through the dissolution into the molten PCM. (b) Series of confocal laser scanning microscope (CLSM) images showing the release of methylene blue at 50 °C (the top panels) and no release at 4 °C (the bottom). (c) Temporal change of absorbance at 664 nm (the left *y*-axis) and the concentration of methylene blue (the right *y*-axis) in the suspension medium at 50 and 4 °C. (d) Temporal change of absorbance at 353 nm (the left *y*-axis), and the concentration of palbociclib isethionate (the right *y*-axis) in the suspension medium at 50, 36.5, and 4 °C. (e) Temporal change of the release rate of palbociclib isethionate at 50, 36.5, and 4 °C.

photothermal effect. It is expected that photothermal heating performance is significantly lowered when the bulk dispersion is directly used as the photothermal agent because the nanoparticles diffuse out in the body. When the aqueous solution of 5 w/w% of PVA without PDA nanoparticles is used, the temperature slightly increases to 33 °C, as shown in the rightmost panel of Figure 2b. The spatial distributions of the temperature increase from the initial for the microcapsules with and without enrichment, the bulk PDA dispersion, and the PVA solution upon the laser irradiation for 12.5 min are summarized in Figure 2c.

The temperature is continuously monitored and averaged for the entire volume in the chamber. The average temperature rapidly increases over time and almost reaches a steady state in 12.5 min for all samples, as shown in Figure 2d. When the laser is off, the average temperature rapidly drops due to cooling by the surrounding. With the temporal changes of the average temperature during the heating and cooling, we estimate the photothermal conversion efficiency, η, of PDA nanoparticles in the core of the microcapsules (see the Supporting Information for the details)

$$\eta = \frac{hA(T_M - T_0) - Q_{solv}}{I(1 - 10^{-Abs})} \quad (1)$$

where h is the heat transfer coefficient, A is the surface area, T_M is the maximum average temperature at a steady state, T_0 is the temperature of the surrounding, Q_{solv} is the photothermal heat of the suspension medium, I is the power of the laser source, and Abs is the absorbance. The value of hA is estimated from the drop of the average temperature when the laser is off, and the value of Q_{solv} is estimated from the steady-state average temperature for the aqueous solution of 5 w/w% of PVA without the microcapsules. The conversion efficiency is estimated as η = 48% for the microcapsules containing 1.3 w/w% of PDA nanoparticles and that is η = 54% for the microcapsules containing 0.17 w/w% of PDA nanoparticles. The bulk dispersion of PDA nanoparticles with a concentration of 0.17 w/w% shows the conversion efficiency of η = 48%, which is comparable with those for the microcapsules. This indicates that the encapsulation and enrichment of PDA nanoparticles in the core of the microcapsules do not degrade the intrinsic photothermal performance of PDA nanoparticles.

https://doi.org/10.1021/acs.chemmater.3c00517
Chem. Mater. XXXX, XXX, XXX−XXX

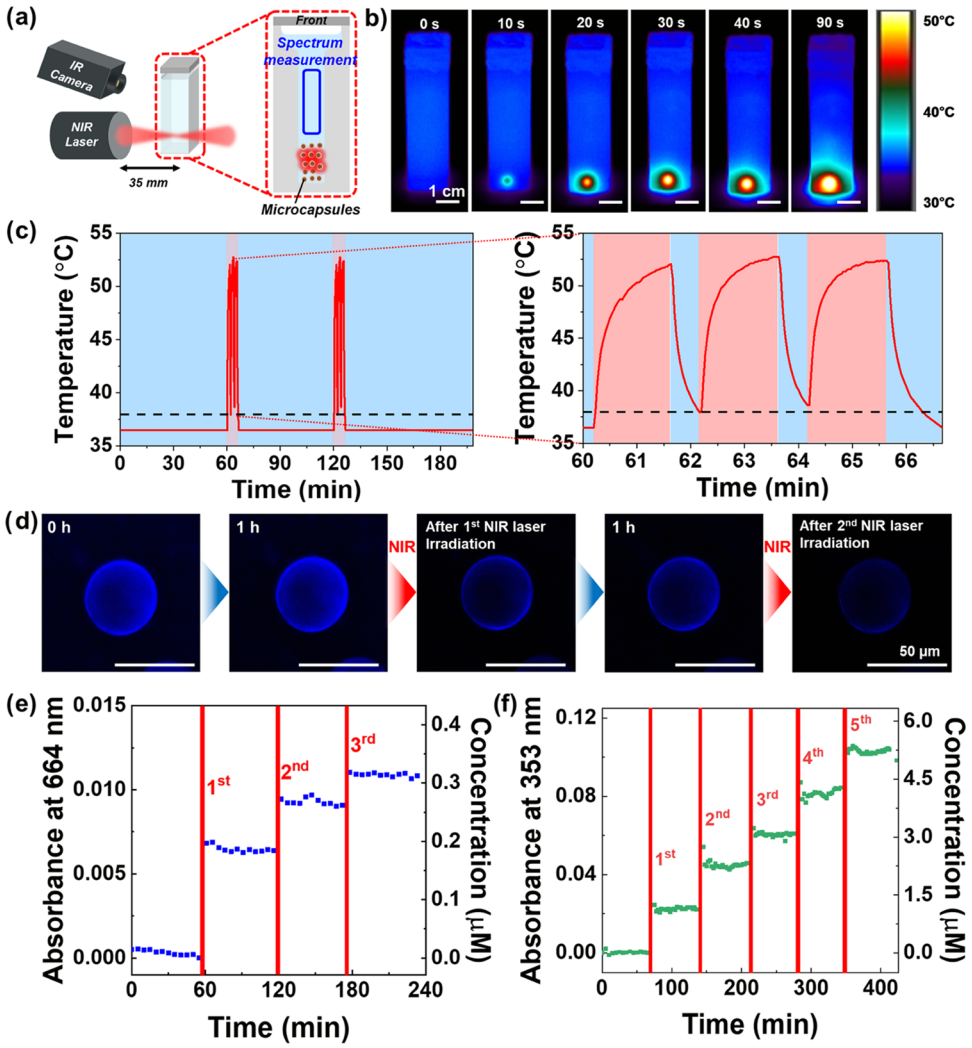

Figure 4. (a) Schematic for the experimental setup to study near-infrared (NIR)-induced heating and drug release. (b) Temporal change of temperature maps during laser irradiation for 90 s. (c) Temporal change of temperature on the position of the laser spot. The sample is heated for 6 min at 60 and 120 min by laser irradiation, where the laser is on for 1.5 min and off for 0.5 min three times. (d) Series of CLSM images showing the laser-induced release of methylene blue. (e) Temporal change of absorbance at 664 nm (the left *y*-axis) and the concentration of methylene blue (the right *y*-axis) in the suspension medium, where the sample is heated by laser irradiation for 6 min at 55, 116, and 172 min. (f) Temporal change of absorbance at 353 nm (the left *y*-axis) and the concentration of palbociclib isethionate (the right *y*-axis) in the suspension medium, where the sample is heated by laser irradiation for 6 min at 65, 135, 205, 275, and 345 min.

2.3. Temperature-Responsive Release of Drugs. The PCM−polymer composite shell of the microcapsules selectively allows the release of molecules that are soluble in the molten PCM.[41] Most small-molecule drugs have limited solubility in water due to their hydrophobic moiety, which makes them partially soluble in 1-tetradecanol. Therefore, various drugs can be released into the surrounding when the temperature increases above the melting point of 38 °C. As the solubility is highly reduced in the frozen PCM, the drugs can be stored in the core at low temperatures. That is, the drug-loaded microcapsules can be stored in a refrigerated state, which can be injected into a body without significant leakage in the short term as the body temperature is slightly lower than the melting point. When the microcapsules are locally heated above the melting point by irradiation with a NIR laser, the drugs are released to the heated regions on demand through the molten PCM nanochannels in the composite shell, as illustrated in Figure 3a. Therefore, the microcapsules potentially provide synergistic chemophotothermal therapy.

We first verify the temperature responsiveness before studying the NIR responsiveness. As a model drug, a fluorescent dye of methylene blue is encapsulated in the core, which allows the direct visualization of the release with a confocal laser scanning microscope (CLSM); the methylene blue has a partition coefficient of 0.92 for molten 1-tetradecanol to water, as shown in Figure S6. Methylene blue is dissolved in the innermost phase of the double-emulsion template at a concentration of 0.25 w/w%, and the microcapsules are produced by following the same protocol of osmotic-pressure-induced enrichment and UV irradiation. The methylene blue is safely stored in the core without leakage at a temperature of 4 °C, below the melting point of 1-tetradecanol, which is released from the microcapsules at a temperature of 50 °C, as shown in Figure 3b. The temperature-dependent rate of the release is also confirmed by the temporal change of the absorbance at 664 nm for the supernatant fluid of the suspension, as shown in Figure 3c. There is a negligible

https://doi.org/10.1021/acs.chemmater.3c00517
Chem. Mater. XXXX, XXX, XXX−XXX

release of methylene blue at 4 °C in a time scale of a day, whereas 73% is released in 10 h at 50 °C.

We also study the temperature-responsive release with an anticancer drug, palbociclib isethionate, which is one of the most promising drugs for the treatment of breast cancers;[42−44] although both palbociclib and palbociclib isethionate are effective anticancer drugs, we choose palbociclib isethionate due to relatively high solubility in water to increase payload. In common, hydrophilicity and solubility of drugs can be enhanced by adjusting pH to render functional groups of the drugs ionized, which potentially helps secure a high payload in the microcapsules. Palbociclib isethionate is dissolved in the innermost phase at a concentration of 0.2 w/w% and enriched by osmosis. Palbociclib isethionate has a partition coefficient of 2.3 as shown in Figure S7, thereby enabling the temperature-responsive release. The release profile is measured using the temporal change of absorbance for the supernatant fluid of the suspension for the drug-laden microcapsules in the bottom of a transparent quartz cuvette, as shown in Figure S8. As palbociclib isethionate shows a characteristic absorbance peak at 353 nm in water and the absorbance is linearly proportional to the concentration as shown in Figure S7, the temporal change of the concentration is directly calculated from that of absorbance, as shown in Figure 3d. The concentration of the drug, $c(t)$, rapidly increases in the early stage and gets gradually saturated over time by following an exponential function

$$c(t) = c_\infty(1 - e^{-t/\tau}) \tag{2}$$

where c_∞ is a final steady-state concentration and τ is a characteristic time scale for the release. The concentration reaches c_∞ = 7.3 μM in 40 h at 50 °C. The value of τ is estimated as 12 h at 50 °C from the fitting. The release is significantly retarded for temperatures of 36.5 and 4 °C. The value of τ is 7.1 days at 36.5 °C and τ = 44 days at 4 °C. That is, it is expected that the drug is slowly released for 3τ of 21 days when the microcapsules are injected and implanted into the body without the NIR irradiation. When the microcapsules are stored at 4 °C, a loss of the drugs is less than 26% up to 15 days. The release rate is estimated by differentiating eq 2

$$\dot{c} = \frac{\mathrm{d}c}{\mathrm{d}t} = \frac{c_\infty}{\tau} e^{-t/\tau} \tag{3}$$

The initial rate is 15 μM/h at 50 °C, which significantly decreases to 0.53 μM/h at 36.5 °C and 0.12 μM/h at 4 °C, as shown in Figure 3e.

2.4. NIR-Responsive Release of Drugs. The release of the drugs can be drastically accelerated by NIR irradiation. To simulate the release from the microcapsules injected in the body, the temperature of the suspension is set to 36.5 °C and the microcapsules at the bottom of the cuvette are irradiated with a NIR laser, as illustrated in Figure 4a. Upon the irradiation, the temperature rapidly increases and reaches 50 °C in 90 s, as shown in Figure 4b. To avoid the excessive increase in the temperature, the laser is cyclically on for 1.5 min and off for 0.5 min to induce NIR-triggered heating and release, as shown in Figure 4c and Movie S4. The temperature increases above the melting point of 1-tetradecanol during the cycling so that the local temperature of the individual microcapsules is expected to be far above the melting point, ensuring the release. For methylene blue, the release is confirmed by the confocal microscope, as shown in Figure 4d. The fluorescence intensity drops when the microcapsules are irradiated by a laser, whereas no change is observed without the irradiation.

The NIR laser-triggered on-demand release is further quantified by the change of absorbance. Methylene blue is released during the cyclic irradiation of 6 min, and the release is stopped when the laser is off, as shown in Figure 4e. It seems that the microcapsules are rapidly cooled below the melting point by the surrounding medium, which remains not significantly heated as the photothermal heating is localized in the microcapsules. Therefore, it is possible to control the release. For example, 66% of methylene blue is released during the first irradiation, and no leakage is observed for the following 60 min without the irradiation. Afterward, 26% of methylene blue is released during the second irradiation. This release on and off can be done until all available methylene blue is released. In the same manner, the release of palbociclib isethionate is controllable with NIR irradiation, as shown in Figure 4f. Approximately 15% of palbociclib isethionate or equivalently about 1.1 μM is released in each period of the NIR irradiation for 6 min. The release is quite consistent for repeated irradiation. The average release rate for each irradiation is approximately 260 μM/d, which is 17 times higher than that at 50 °C in Figure 3e. This fast release during the NIR irradiation is attributed to the very high temperature of the individual microcapsules due to the localized photothermal heating. The microcapsules remain unchanged, without any breakage or nanoparticle aggregation, after repeated laser irradiation, as shown in Figure S9. Also, the microcapsules show high chemical stability as the shells are made of cross-linked polymers whose backbone is free from hydrolysis; no degradation of the shells is observed for long-term storage at high temperature, as shown in Figure S10. The encapsulation efficiency of methylene blue and palbociclib isethionate is calculated as 82 and 84%, respectively, from the concentrations estimated from the absorbance and initial loading of the molecules in the innermost phase of the double-emulsion droplets by considering the volume shrinkage by osmotic compression and the dilution of the molecules by the release.

3. CONCLUSIONS

In this work, we design smart microcapsules for on-demand local heating and drug release triggered by NIR irradiation. As a template, W/O/W double-emulsion droplets are produced to have an ultrathin shell by a capillary microfluidic device. The middle oil phase is composed of a photocurable monomer, PCM, and a molecular compatibilizer, which turns into a polymer−PCM composite by photopolymerization of the monomer, where PCM forms continuous nanochannels in the polymer framework, serving as routes for transmembrane transport of molecules at the molten state. The inner water phase contains PDA nanoparticles, which provide a high efficiency of photothermal conversion. To render the microcapsules to have small sizes and high concentrations of PDA nanoparticles and drugs, the double-emulsion droplets are significantly shrunken by *in situ* osmotic extraction of water by applying hypertonic stress. The resulting microcapsules show a high performance of photothermal heating for NIR laser irradiation owing to concentrated PDA nanoparticles in the core. At the same time, the microcapsules safely store drugs in the core at low temperatures and release them in a controlled manner when the temperature is increased above the melting

https://doi.org/10.1021/acs.chemmater.3c00517
Chem. Mater. XXXX, XXX, XXX−XXX

point of PCM. The NIR-triggered release of the anticancer drugs along with the localized photothermal heating potentially provides a synergistic chemophotothermal therapy of cancers. As the microcapsules with a diameter of 38 μm are small enough to be injected through a needle and large enough to be implanted in the tissues, they can be introduced and immobilized to the cancer sites. More importantly, the photothermal PDA nanoparticles do not diffuse out in the body as they are safely confined in the core of the microcapsules, so high photothermal performance is expected. As the shell components of 1-tetradecanol and *p*(ETPTA-*co*-LA) are generally nontoxic as long as unreacted monomers are completely removed,[45] the microcapsules show a high cell viability, as shown in Figure S11. Therefore, we will investigate the performance of our microcapsules as a synergistic chemophotothermal agent with animal models in a follow-up study.

4. EXPERIMENTAL SECTION

4.1. Synthesis of Polydopamine−Melanin Core−Shell Nanoparticles. Polydopamine nanoparticles with an average diameter of 100 nm were first synthesized by the oxidative polymerization of dopamine by following the protocol previously reported.[46−48] The melanin shell was coated on the polydopamine nanoparticles by self-oxidation. A 100 mg of 3,4-dihydroxy-L-phenylalanine (L-DOPA, Sigma-Aldrich) was dissolved in 50 mL of distilled water, which was injected into 150 mL of 0.02 w/w% aqueous dispersion of polydopamine nanoparticles in a round flask by using a syringe pump (Legato 100, KD Scientific) with a flow rate of 12.5 mL/h for 4 h. Afterward, 530 μL of 1 M NaOH solution was injected into the mixture and stirred at room temperature for 18 h. The resulting polydopamine−melanin core−shell nanoparticles were purified with distilled water five times.

4.2. Preparation of Capillary Microfluidic Devices. The capillary microfluidic devices were prepared by slightly modifying the protocol that was previously reported.[38−40] Two cylindrical capillaries (0.58 mm of inner diameter, 1.00 mm of outer diameter, World Precision Instruments) were tapered using a capillary puller (P97, Sutter Instruments), and their tips were sanded to have diameters of 80 and 120 μm, respectively; these capillaries were used for the injection of fluids and collection of drops, respectively. The inner volume of the injection capillary with an 80 μm diameter orifice was infiltrated with n-octadecyl trimethoxysilane (Gelest) and incubated for 20 min to render the inner wall hydrophobic. Afterward, the capillary was dipped into 2-[methoxy(polyethyleneoxy)propyl]-trimethoxysilane (Gelest) for 20 min to render the outer surface hydrophilic while blowing with nitrogen through an untapered opening to avoid the invasion of the liquid into the inner space. The entire surface of the collection capillary with a 120 μm diameter orifice was treated with 2-[methoxy(polyethyleneoxy)propyl]-trimethoxysilane for 20 min. After the surface treatment, the capillaries were rinsed with isopropanol and distilled water and fully dried. The injection and collection capillaries were coaxially assembled in a square-shaped capillary (1.05 mm of inner diameter, 1.50 mm of outer diameter, Atlantic International Technologies) under observation with an optical microscopy. The separation between the two tips was set to be 100 μm. One cylindrical capillary was manually tapered, which was inserted into the untapered opening of the capillary with an 80 μm diameter orifice. To inject fluids into the device, all junction parts were encased with upside-down needles and completely sealed by using epoxy glue. The untapered opening of the collection capillary was connected with a 4 m long polyethylene tubing (0.86 mm of inner diameter, 1.32 mm of outer diameter, Scientific Commodities).

4.3. Preparation and Characterization of Microcapsules. As an innermost phase of the double-emulsion template, polydopamine−melanin core−shell nanoparticles were dispersed at a concentration of 0.17 w/w% in 5 w/w% of aqueous solution of poly(vinyl alcohol) (PVA, M_w 13,000−23,000, Sigma-Aldrich). As a model drug, methylene blue (Sigma-Aldrich) was dissolved in the innermost phase at a concentration of 0.25 w/w%. For encapsulation of the anticancer drug, 0.2 w/w% of palbociclib isethionate (Sigma-Aldrich) was dissolved in the innermost phase. The middle oil phase was a mixture of 29 w/w% 1-tetradecanol (Sigma-Aldrich), 35 w/w% lauryl acrylate (Sigma-Aldrich), 35 w/w% trimethylolpropane ethoxylate triacrylate (ETPTA, M_n 428, Sigma-Aldrich), and 1 w/w% 2-hydroxy-2-methylpropiophenone (Darocur 1173, Sigma-Aldrich). The continuous phase was an aqueous solution of 10 w/w% PVA and 250 mM NaCl with an osmolarity of 600 mOsmol/L. The innermost, middle, and continuous phases were simultaneously injected into the small tapered capillary, the injection capillary, and the interstice between the injection capillary and the square capillary by using syringe pumps. The flow rates were set to 350, 650, and 3500 μL/h, respectively. The temperature was maintained at 50 °C during the operation. The drops from the 4 m long tubing were collected in a glass vial containing an aqueous solution of 1 w/w% PVA and 300 mM NaCl with an osmolarity of 600 mOsmol/L, at which they were continuously irradiated by UV (Inno cure 100N, Lichtzen). The resulting microcapsules were washed with cold distilled water and stored at 4°C.

4.4. Characterization. The polydopamine and melanin-coated polydopamine nanoparticles were observed with scanning electron microscopy (SEM, SU8230, Hitachi) after osmium coating. For surface charge characterization, dynamic light scattering (DLS, Zetasizer Nano ZS90, Malvern) was used. The formation and flow of emulsion droplets were observed using an inverted microscope (Eclipse TS100, Nikon) equipped with a high-speed CMOS camera (MotionScope M3, Redlake). The microcapsules suspended in water were observed with optical microscopies (Eclipse Ti-U and L150, Nikon) equipped with a heating stage (T96-PE, Linkam). The surface and cross section of the shell membrane were observed with SEM (S-4800, Hitachi) after washing out 1-tetradecanol using isopropanol and coating with 5 nm thick osmium tetroxide. To characterize the photothermal effect, the aqueous suspension of microcapsules was loaded into a circular imaging chamber with a diameter of 13 mm and a height of 0.12 mm (Grace Bio-Labs SecureSeal imaging spacer, Sigma-Aldrich) sandwiched by two glass slides. The chambers were irradiated with a NIR laser (LVI Technology) with a wavelength of 808 nm, an intensity of 650 mW, and a spot diameter of 2.5 mm for 750 s from a distance of 35 mm, during which the temperature was recorded every 2 s using a thermal imaging camera (Infrared camera, A325sc, FLIR). The absorbance was measured by using a microplate reader (Infinite M200 Pro, Tecan). To study release behavior, 1.3 mL of aqueous suspensions of methylene blue or palbociclib isethionate-laden microcapsules were loaded into a microcell with a maximum loading of 1.4 mL and the beam path of 1 cm (Quartz SUPRASIL, Hellma). To prevent undesired evaporation of water during the long-term release study at a high temperature, the cuvette was closed with a lid and tightly sealed with parafilm. To control the temperature, a water circulator (AD-RC08i, BNC Korea) was used. The absorbance spectra of the media were measured using a UV−vis spectrophotometer (UV-1900, Shimadzu). To study laser-triggered release, the microcapsules located at the bottom of the microcells were repetitively irradiated with the NIR laser for 3 cycles, where the laser was on for 90 s and off for 30 s for each cycle. During the laser irradiation, temperature was monitored using the thermal imaging camera. To visualize the release of methylene blue, a confocal microscope (LSM 5 PASCAL, Zeiss) was used with a laser of 633 nm.

■ ASSOCIATED CONTENT

Supporting Information

The Supporting Information is available free of charge at https://pubs.acs.org/doi/10.1021/acs.chemmater.3c00517.

Calculation of the photothermal conversion efficiency, scanning electron microscope (SEM) images of polydopamine nanoparticles, optical microscope (OM)

https://doi.org/10.1021/acs.chemmater.3c00517
Chem. Mater. XXXX, XXX, XXX−XXX

image of aggregated melanin@polydopamine nanoparticles by centrifugation, image of spontaneous separation of microcapsules from large solid beads, OM images of microcapsules produced without and with osmosis, OM images of microcapsule arrays for photothermal experiment, measurement of partition coefficients, image of microcapsules in a cuvette, OM image of microcapsules with a high stability, cell viability, and movie descriptions (PDF)

The microfluidic production and the shrinkage of water-in-oil-in-water (W/O/W) double-emulsion droplets with an ultrathin shell (MP4)

The microcapsules showing a reversible change of states depending on temperature (MP4)

The temperature distribution in a chamber containing microcapsules under an 808 nm laser irradiation monitored with an infrared (IR) camera (MP4)

Temperature change of a microcapsule-laden cuvette under an 808 nm laser irradiation for 90 s and cooling for 30 s (MP4)

AUTHOR INFORMATION

Corresponding Authors

Jaemoon Yang − *Department of Radiology, College of Medicine, Yonsei University, Seoul 03722, Republic of Korea;* orcid.org/0000-0001-7365-0395; Email: sysmolray@yonsei.ac.kr

Shin-Hyun Kim − *Department of Chemical and Biomolecular Engineering, Korea Advanced Institute of Science and Technology (KAIST), Daejeon 34141, Republic of Korea;* orcid.org/0000-0003-4095-5779; Email: kim.sh@kaist.ac.kr

Authors

Ji-Won Kim − *Department of Chemical and Biomolecular Engineering, Korea Advanced Institute of Science and Technology (KAIST), Daejeon 34141, Republic of Korea;* Present Address: Department of Chemistry, The University of Texas at Austin, Austin, Texas 78712, United States (J.W.K.)

Sang Hoon Han − *Department of Chemical and Biomolecular Engineering, Korea Advanced Institute of Science and Technology (KAIST), Daejeon 34141, Republic of Korea;* Present Address: Samsung Electronics, Yongin 17113, Republic of Korea (S.H.H.).

Minhee Ku − *Department of Radiology, College of Medicine, Yonsei University, Seoul 03722, Republic of Korea*

Complete contact information is available at: https://pubs.acs.org/10.1021/acs.chemmater.3c00517

Author Contributions

⊥J.-W.K., S.H.H., and M.K. contributed equally to this work. The manuscript was written through contributions of all authors. All authors have given approval to the final version of the manuscript.

Funding

This work was supported by the National Research Foundation funded by the Ministry of Science and ICT.

Notes

The authors declare no competing financial interest.

ACKNOWLEDGMENTS

This work was supported by the National Research Foundation (NRF) (NRF-2020R1A2C2003245 and 2021R1A2C1009894) funded by the Ministry of Science and ICT.

ABBREVIATIONS

W/O/W, water-in-oil-in-water; PCM, phase-change material; NIR, near-infrared; PDA, polydopamine; PVA, poly(vinyl alcohol); ETPTA, trimethylolpropane ethoxylate triacrylate; LA, lauryl acrylate; UV, ultraviolet; IR, infrared; CLSM, confocal laser scanning microscope; SEM, scanning electron microscopy; OM, optical microscope

REFERENCES

(1) Cheng, L.; Wang, C.; Feng, L. Z.; Yang, K.; Liu, Z. Functional Nanomaterials for Phototherapies of Cancer. *Chem. Rev.* **2014**, *114*, 10869−10939.

(2) Huang, X. H.; El-Sayed, I. H.; Qian, W.; El-Sayed, M. A. Cancer cell imaging and photothermal therapy in the near-infrared region by using gold nanorods. *J. Am. Chem. Soc.* **2006**, *128*, 2115−2120.

(3) Choi, W. I.; Kim, J. Y.; Kang, C.; Byeon, C. C.; Kim, Y. H.; Tee, G. Tumor Regression In Vivo by Photothermal Therapy Based on Gold-Nanorod-Loaded, Functional Nanocarriers. *ACS Nano* **2011**, *5*, 1995−2003.

(4) Ren, F.; Bhana, S.; Norman, D. D.; Johnson, J.; Xu, L. J.; Baker, D. L.; Parrill, A. L.; Huang, X. H. Gold Nanorods Carrying Paclitaxel for Photothermal-Chemotherapy of Cancer. *Bioconjugate Chem.* **2013**, *24*, 376−386.

(5) Jeong, W. C.; Kim, S. H.; Yang, S. M. Photothermal Control of Membrane Permeability of Microcapsules for On-Demand Release. *ACS Appl. Mater. Interfaces* **2014**, *6*, 826−832.

(6) Hauck, T. S.; Jennings, T. L.; Yatsenko, T.; Kumaradas, J. C.; Chan, W. C. W. Enhancing the Toxicity of Cancer Chemotherapeutics with Gold Nanorod Hyperthermia. *Adv. Mater.* **2008**, *20*, 3832−3838.

(7) Huang, X. H.; Jain, P. K.; El-Sayed, I. H.; El-Sayed, M. A. Plasmonic photothermal therapy (PPTT) using gold nanoparticles. *Laser Med. Sci.* **2008**, *23*, 217−228.

(8) Moon, H. K.; Lee, S. H.; Choi, H. C. In Vivo Near-Infrared Mediated Tumor Destruction by Photothermal Effect of Carbon Nanotubes. *ACS Nano* **2009**, *3*, 3707−3713.

(9) Yang, K.; Zhang, S. A.; Zhang, G. X.; Sun, X. M.; Lee, S. T.; Liu, Z. A. Graphene in Mice: Ultrahigh In Vivo Tumor Uptake and Efficient Photothermal Therapy. *Nano Lett.* **2010**, *10*, 3318−3323.

(10) Robinson, J. T.; Tabakman, S. M.; Liang, Y. Y.; Wang, H. L.; Casalongue, H. S.; Vinh, D.; Dai, H. J. Ultrasmall Reduced Graphene Oxide with High Near-Infrared Absorbance for Photothermal Therapy. *J. Am. Chem. Soc.* **2011**, *133*, 6825−6831.

(11) Akhavan, O.; Ghaderi, E.; Aghayee, S.; Fereydooni, Y.; Talebi, A. The use of a glucose-reduced graphene oxide suspension for photothermal cancer therapy. *J. Mater. Chem.* **2012**, *22*, 13773−13781.

(12) Yang, K.; Wan, J. M.; Zhang, S.; Tian, B.; Zhang, Y. J.; Liu, Z. The influence of surface chemistry and size of nanoscale graphene oxide on photothermal therapy of cancer using ultra-low laser power. *Biomaterials* **2012**, *33*, 2206−2214.

(13) Cheon, Y. A.; Bae, J. H.; Chung, B. G. Reduced Graphene Oxide Nanosheet for Chemo-photothermal Therapy. *Langmuir* **2016**, *32*, 2731−2736.

(14) Thakur, M.; Kumawat, M. K.; Srivastava, R. Multifunctional graphene quantum dots for combined photothermal and photodynamic therapy coupled with cancer cell tracking applications. *RSC Adv.* **2017**, *7*, 5251−5261.

(15) Wang, H.; Mu, Q. X.; Wang, K.; Revia, R. A.; Yen, C.; Gu, X. Y.; Tian, B. W.; Liu, J.; Zhang, M. Q. Nitrogen and boron dual-doped

graphene quantum dots for near-infrared second window imaging and photothermal therapy. *Appl. Mater. Today* **2019**, *14*, 108−117.
(16) Li, S. H.; Zhou, S. X.; Li, Y. C.; Li, X. H.; Zhu, J.; Fan, L. Z.; Yang, S. H. Exceptionally High Payload of the IR780 Iodide on Folic Acid-Functionalized Graphene Quantum Dots for Targeted Photothermal Therapy. *ACS Appl. Mater. Interfaces* **2017**, *9*, 22332−22341.
(17) Zhu, Z. J.; Su, M. Polydopamine Nanoparticles for Combined Chemo- and Photothermal Cancer Therapy. *Nanomaterials* **2017**, *7*, No. 160.
(18) Poinard, B.; Neo, S. Z. Y.; Yeo, E. L. L.; Heng, H. P. S.; Neoh, K. G.; Kah, J. C. Y. Polydopamine Nanoparticles Enhance Drug Release for Combined Photodynamic and Photothermal Therapy. *ACS Appl. Mater. Interfaces* **2018**, *10*, 21125−21136.
(19) Qiu, J. C.; Shi, Y. F.; Xia, Y. N. Polydopamine Nanobottles with Photothermal Capability for Controlled Release and Related Applications. *Adv. Mater.* **2021**, *33*, No. 2104729.
(20) Liu, Y. L.; Ai, K. L.; Liu, J. H.; Deng, M.; He, Y. Y.; Lu, L. H. Dopamine-Melanin Colloidal Nanospheres: An Efficient Near-Infrared Photothermal Therapeutic Agent for In Vivo Cancer Therapy. *Adv. Mater.* **2013**, *25*, 1353−1359.
(21) Wang, X. Y.; Zhang, J. S.; Wang, Y. T.; Wang, C. P.; Xiao, J. R.; Zhang, Q.; Cheng, Y. Y. Multi-responsive photothermal-chemotherapy with drug-loaded melanin-like nanoparticles for synergetic tumor ablation. *Biomaterials* **2016**, *81*, 114−124.
(22) Cheng, W.; Zeng, X. W.; Chen, H. Z.; Li, Z. M.; Zeng, W. F.; Mei, L.; Zhao, Y. L. Versatile Polydopamine Platforms: Synthesis and Promising Applications for Surface Modification and Advanced Nanomedicine. *ACS Nano* **2019**, *13*, 8537−8565.
(23) Yang, J.; Choi, J.; Bang, D.; Kim, E.; Lim, E. K.; Park, H.; Suh, J. S.; Lee, K.; Yoo, K. H.; Kim, E. K.; et al. Convertible Organic Nanoparticles for Near-Infrared Photothermal Ablation of Cancer Cells. *Angew. Chem., Int. Ed.* **2011**, *50*, 441−444.
(24) Zhou, J.; Lu, Z. G.; Zhu, X. J.; Wang, X. J.; Liao, Y.; Ma, Z. F.; Li, F. Y. NIR photothermal therapy using polyaniline nanoparticles. *Biomaterials* **2013**, *34*, 9584−9592.
(25) Jiang, B. P.; Zhang, L.; Zhu, Y.; Shen, X. C.; Ji, S. C.; Tan, X. Y.; Cheng, L.; Liang, H. Water-soluble hyaluronic acid-hybridized polyaniline nanoparticles for effectively targeted photothermal therapy. *J. Mater. Chem. B* **2015**, *3*, 3767−3776.
(26) Yslas, E. I.; Ibarra, L. E.; Molina, M. A.; Rivarola, C.; Barbero, C. A.; Bertuzzi, M. L.; Rivarola, V. A. Polyaniline nanoparticles for near-infrared photothermal destruction of cancer cells. *J. Nanopart. Res.* **2015**, *17*, No. 389.
(27) Wang, J. P.; Yan, R.; Guo, F.; Yu, M.; Tan, F. P.; Li, N. Targeted lipid-polyaniline hybrid nanoparticles for photoacoustic imaging guided photothermal therapy of cancer. *Nanotechnology* **2016**, *27*, No. 285102.
(28) Tian, Q. W.; Li, Y. P.; Jiang, S. S.; An, L.; Lin, J. M.; Wu, H. X.; Huang, P.; Yang, S. P. Tumor pH-Responsive Albumin/Polyaniline Assemblies for Amplified Photoacoustic Imaging and Augmented Photothermal Therapy. *Small* **2019**, *15*, No. 1902926.
(29) Chen, M.; Fang, X. L.; Tang, S. H.; Zheng, N. F. Polypyrrole nanoparticles for high-performance in vivo near-infrared photothermal cancer therapy. *Chem. Commun.* **2012**, *48*, 8934−8936.
(30) Yang, K.; Xu, H.; Cheng, L.; Sun, C. Y.; Wang, J.; Liu, Z. In Vitro and In Vivo Near-Infrared Photothermal Therapy of Cancer Using Polypyrrole Organic Nanoparticles. *Adv. Mater.* **2013**, *25*, 945.
(31) Wang, X. J.; Li, H. C.; Liu, X. P.; Tian, Y.; Guo, H. S.; Jiang, T.; Luo, Z. M.; Jin, K.; Kuai, X. P.; Liu, Y.; et al. Enhanced photothermal therapy of biomimetic polypyrrole nanoparticles through improving blood flow perfusion. *Biomaterials* **2017**, *143*, 130−141.
(32) Wang, X.; Ma, Y. C.; Sheng, X.; Wang, Y. C.; Xu, H. X. Ultrathin Polypyrrole Nanosheets via Space-Confined Synthesis for Efficient Photothermal Therapy in the Second Near-Infrared Window. *Nano Lett.* **2018**, *18*, 2217−2225.
(33) Nam, J.; Son, S.; Ochyl, L. J.; Kuai, R.; Schwendeman, A.; Moon, J. J. Chemo-photothermal therapy combination elicits anti-tumor immunity against advanced metastatic cancer. *Nat. Commun.* **2018**, *9*, No. 1074.
(34) Baek, S.; Singh, R. K.; Khanal, D.; Patel, K. D.; Lee, E. J.; Leong, K. W.; Chrzanowski, W.; Kim, H. W. Smart multifunctional drug delivery towards anticancer therapy harmonized in mesoporous nanoparticles. *Nanoscale* **2015**, *7*, 14191−14216.
(35) Sharma, H.; Mondal, S. Functionalized Graphene Oxide for Chemotherapeutic Drug Delivery and Cancer Treatment: A Promising Material in Nanomedicine. *Int. J. Mol. Sci.* **2020**, *21*, No. 6280.
(36) Gao, Y.; Zhong, S. L.; Xu, L. F.; He, S. H.; Dou, Y. M.; Zhao, S. N.; Chen, P.; Cui, X. J. Mesoporous silica nanoparticles capped with graphene quantum dots as multifunctional drug carriers for photothermal and redox-responsive release. *Microporous Mesoporous Mater.* **2019**, *278*, 130−137.
(37) Lei, W.; Sun, C. S.; Jiang, T. Y.; Gao, Y. K.; Yang, Y.; Zhao, Q. F.; Wang, S. L. Polydopamine-coated mesoporous silica nanoparticles for multi-responsive drug delivery and combined chemo-photothermal therapy. *Mat. Sci. Eng. C* **2019**, *105*, No. 110103.
(38) Utada, A. S.; Lorenceau, E.; Link, D. R.; Kaplan, P. D.; Stone, H. A.; Weitz, D. A. Monodisperse double emulsions generated from a microcapillary device. *Science* **2005**, *308*, 537−541.
(39) Kim, S. H.; Kim, J. W.; Cho, J. C.; Weitz, D. A. Double-emulsion drops with ultra-thin shells for capsule templates. *Lab Chip* **2011**, *11*, 3162−3166.
(40) Choi, Y. H.; Hwang, J. S.; Han, S. H.; Lee, C. S.; Jeon, S. J.; Kim, S. H. Thermo-Responsive Microcapsules with Tunable Molecular Permeability for Controlled Encapsulation and Release. *Adv. Funct. Mater.* **2021**, *31*, No. 2100782.
(41) Kim, J. W.; Lee, S. S.; Park, J.; Ku, M.; Yang, J.; Kim, S. H. Smart Microcapsules with Molecular Polarity- and Temperature-Dependent Permeability. *Small* **2019**, *15*, No. 1900434.
(42) Turner, N. C.; Ro, J.; Andre, F.; Loi, S.; Verma, S.; Iwata, H.; Harbeck, N.; Loibl, S.; Bartlett, C. H.; Zhang, K.; et al. Palbociclib in Hormone-Receptor-Positive Advanced Breast Cancer. *New Engl. J. Med.* **2015**, *373*, 209−219.
(43) Harada, M.; Morikawa, M.; Ozawa, T.; Kobayashi, M.; Tamura, Y.; Takahashi, K.; Tanabe, M.; Tada, K.; Seto, Y.; Miyazono, K.; Koinuma, D. Palbociclib enhances activin-SMAD-induced cytostasis in estrogen receptor-positive breast cancer. *Cancer Sci.* **2019**, *110*, 209−220.
(44) Plett, R.; Mellor, P.; Kendall, S.; Hammond, S. A.; Boulet, A.; Plaza, K.; Vizeacoumar, F. S.; Vizeacoumar, F. J.; Anderson, D. H. Homoharringtonine demonstrates a cytotoxic effect against triple-negative breast cancer cell lines and acts synergistically with paclitaxel. *Sci. Rep.* **2022**, *12*, No. 15663.
(45) Moon, H. J.; Ku, M.; Roh, Y. H.; Lee, H. J.; Yang, J.; Bong, K. W. Elimination of Unreacted Acrylate Double Bonds in the Polymer Networks of Microparticles Synthesized via Flow Lithography. *Langmuir* **2020**, *36*, 2271−2277.
(46) Cho, S.; Kim, S. H. Hydroxide ion-mediated synthesis of monodisperse dopamine-melanin nanospheres. *J. Colloid Interface Sci.* **2015**, *458*, 87−93.
(47) Cho, S.; Shim, T. S.; Kim, J. H.; Kim, D. H.; Kim, S. H. Selective Coloration of Melanin Nanospheres through Resonant Mie Scattering. *Adv. Mater.* **2017**, *29*, No. 1700256.
(48) Lee, G. H.; Han, S. H.; Kim, J. B.; Kim, J. H.; Lee, J. M.; Kim, S. H. Colloidal Photonic Inks for Mechanochromic Films and Patterns with Structural Colors of High Saturation. *Chem. Mater.* **2019**, *31*, 8154−8162.

https://doi.org/10.1021/acs.chemmater.3c00517
Chem. Mater. XXXX, XXX, XXX−XXX

Supporting Information

Smart Microcapsules designed for On-demand Local Heating and Drug Release

Ji-Won Kim[a†‡], *Sang Hoon Han*[a†‡], *Minhee Ku*[b‡], *Jaemoon Yang*[b*], *and Shin-Hyun Kim*[a*]

[a]Department of Chemical and Biomolecular Engineering, Korea Advanced Institute of Science and Technology (KAIST), Daejeon 34141, Republic of Korea

[b]Department of Radiology, College of Medicine, Yonsei University, Seoul 03722, Republic of Korea

Contents

S1. Calculation of the photothermal conversion efficiency

S2. Polydopamine nanoparticles

S3. Aggregation of melanin@polydopamine nanoparticles by centrifugation

S4. Spontaneous separation of microcapsules from large solid beads

S5. Microcapsules produced without and with osmosis

S6. Microcapsule arrays for photothermal experiment

S7. Measurement of partition coefficients

S8. Microcapsules in cuvette

S9. High stability of microcapsules

S10. Biocompatibility of microcapsules

S11. Movie descriptions

S1. Calculation of the photothermal conversion efficiency

Temperature, $T(r, t)$, is averaged over the entire volume of water in the well:

$$T(t) = \frac{1}{\pi R^2}\int_0^R 2\pi r T(r,t) dr, \quad (1)$$

where R is the radius of the well. To calculate photothermal conversion efficiency, we consider the energy balance:

$$mC_P \frac{dT}{dt} = Q_{mc} + Q_{solv} - Q_{loss}, (2)$$

where m and C_P are the total mass of water in the well and heat capacity (m = 0.016 g and C_P = 4.184 J g^{-1} °C^{-1}) and Q_{mc}, Q_{solv}, and Q_{loss} are photothermal heating by microcapsules, photothermal heating by water, and energy loss to the surrounding, respectively. The photothermal heating by microcapsules is expressed as

$$Q_{mc} = I(1 - 10^{-Abs})\eta, (3)$$

where I is laser power (I = 650 mW), Abs is absorbance, and η is conversion efficiency. The heat loss is expressed as

$$Q_{loss} = hA\Delta T = hA(T - T_0), (4)$$

where h is the heat transfer coefficient, A is the surface area, and T_0 is the temperature of the surrounding.

At steady state under laser irradiation, equation (2), combined with equations (2) and (3), is simplified into

$$0 = I(1 - 10^{-Abs})\eta + Q_{solv} - hA(T_M - T_0) \text{ or equivalently } \eta = \frac{hA(T_M - T_0) - Q_{solv}}{I(1 - 10^{-Abs})}, (5)$$

where T_M is the maximum average temperature. The value of hA is estimated from the temperature drop during the cooling when the laser is off:

$$mC_P \frac{dT}{dt} = -hA(T - T_0). (6)$$

By integrating equation (6), we obtain

$$\ln\left(\frac{T - T_0}{T_M - T_0}\right) = -\frac{hA}{mC_P}t. (7)$$

Therefore, the value of hA is extracted from $T(t)$ for the cooling without laser irradiation, which is hA = 1.6 mW ˚C^{-1}. The value of Q_{solv} is estimated from the steady-state average temperature of water without microcapsules:

$$0 = Q_{\mathrm{solv}} - hA(T_{\mathrm{M}} - T_0). \quad (8)$$

The value of Q_{solv} is 8.0 mW. Therefore, the values of η are estimated as η = 0.48 for the arrays of microcapsules with enrichment, η = 0.54 for the arrays of microcapsules without enrichment, and η = 0.48 for the bulk PDA dispersion using equation (5) from the values of T_{M}, where the absorbance is measured separately; Abs = 0.043 for the arrays of microcapsules with enrichment, Abs = 0.024 for the arrays of microcapsules without enrichment, and Abs = 0.045 for the bulk PDA dispersion.

S2. Polydopamine nanoparticles

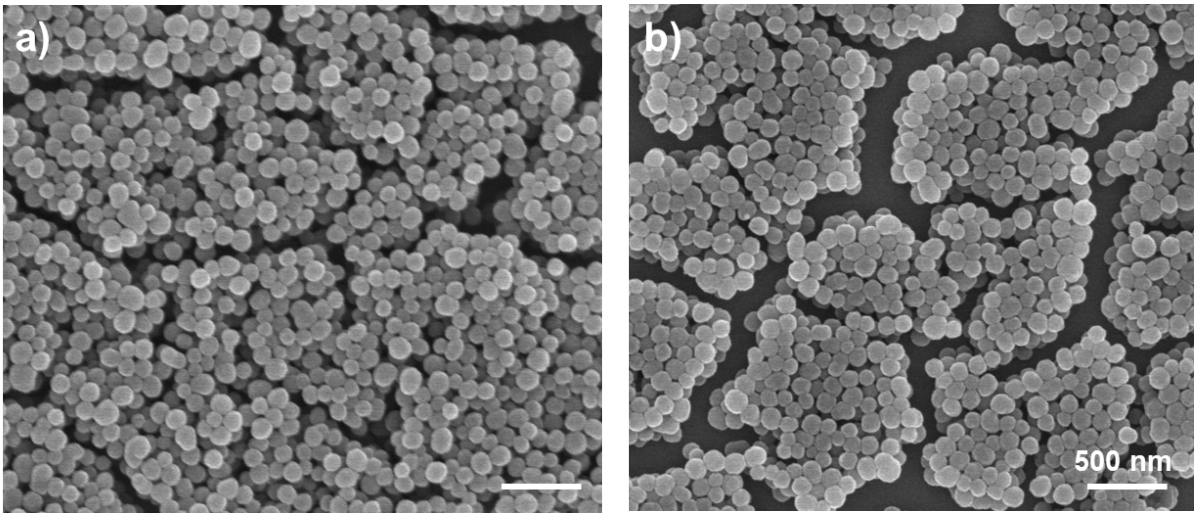

Figure S1. Scanning electron microscope (SEM) images of (a) polydopamine nanoparticles (diameter: 102 nm, Zeta potential: −36 mV) and (b) melanin-coated polydopamine nanoparticles (diameter: 103 nm, Zeta potential: −60 mV)

S3. Aggregation of melanin@polydopamine nanoparticles by centrifugation

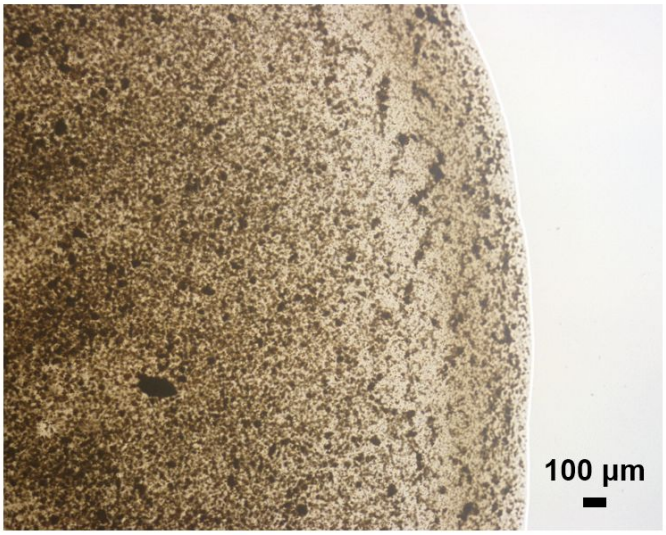

Figure S2. Transmission optical microscope image of aggregated melanin-coated polydopamine nanoparticles at a high concentration.

S4. Spontaneous separation of microcapsules from large solid beads

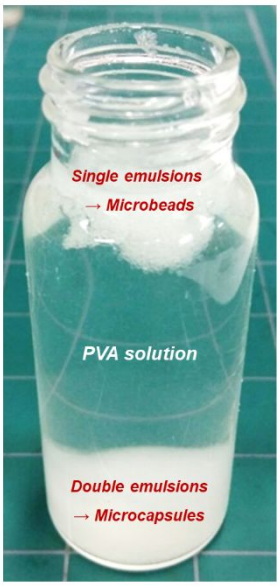

Figure S3. Photograph of suspensions containing both microcapsules and beads. The beads lighter than water float, whereas the microcapsules heavier than water sink.

S5. Microcapsules produced without and with osmosis

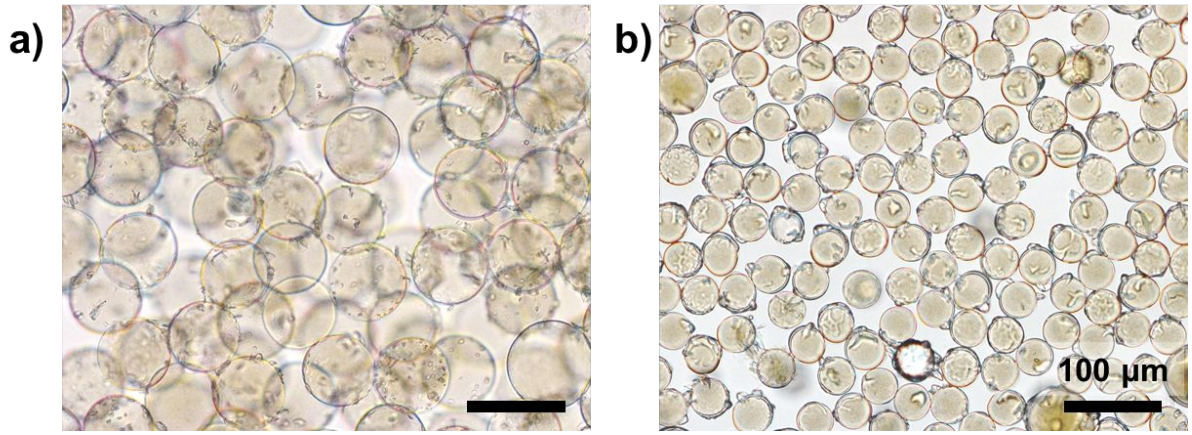

Figure S4. (a, b) Transmission optical microscope images of the microcapsules produced without (a) and with (a) enrichment through osmosis.

S6. Microcapsule arrays for photothermal experiment

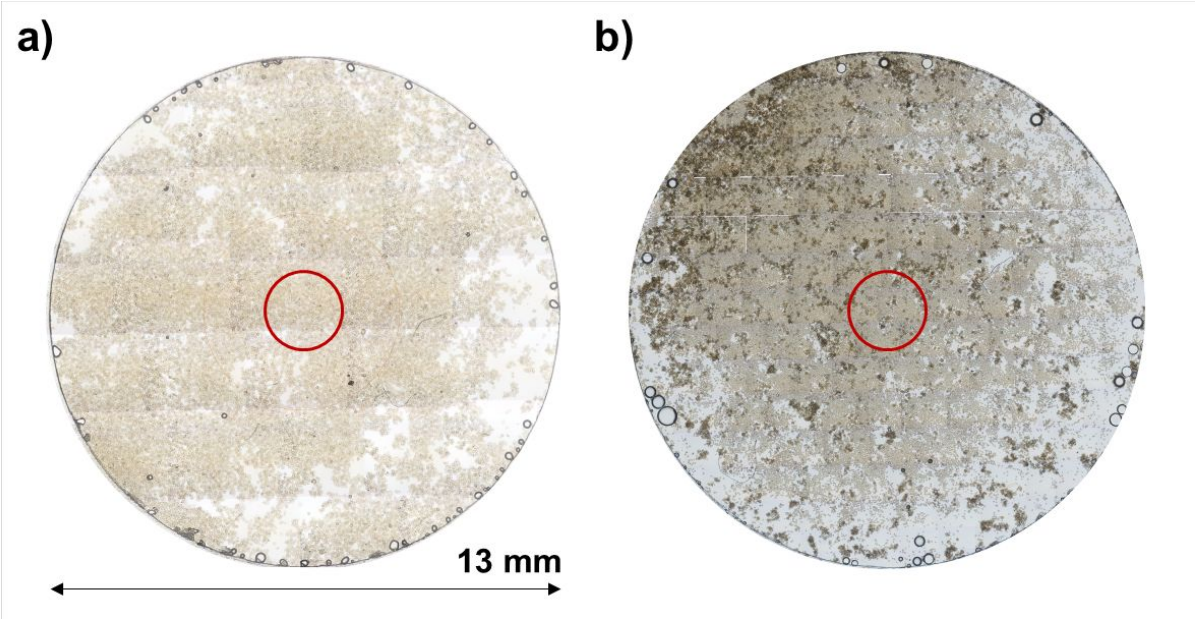

Figure S5. Images of the chambers containing a monolayer of microcapsules produced without (a) and with (b) osmosis-induced enrichment, where the images are prepared by stitching transmission optical microscope images. The diameter of the chamber is 13 mm and the area for the laser irradiation is denoted with a small red circle in the middle.

S7. Measurement of partition coefficients

To measure partition coefficients of methylene blue and palbociclib isethionate, the relationships between absorbance and concentration in water and 1-tetradecanol are first established as standard curves, as shown in Figure S6a-d and S7a-d. After incubating the mixture of water and 1-tetradecanol containing either methylene blue or palbociclib isethionate at 50˚C for a day, water phase and 1-tetradecanol phase are separated, from which absorbance spectra are measured, as shown in Figure S6e and S7e. From the spectra, the concentration in each phase is estimated using the standard curves and the partition coefficient is calculated as the concentration ratio of methylene blue and palbociclib isethionate in 1-tetradecanol to water, $c_{\text{1-tetradecanol}}/c_{\text{water}}$.

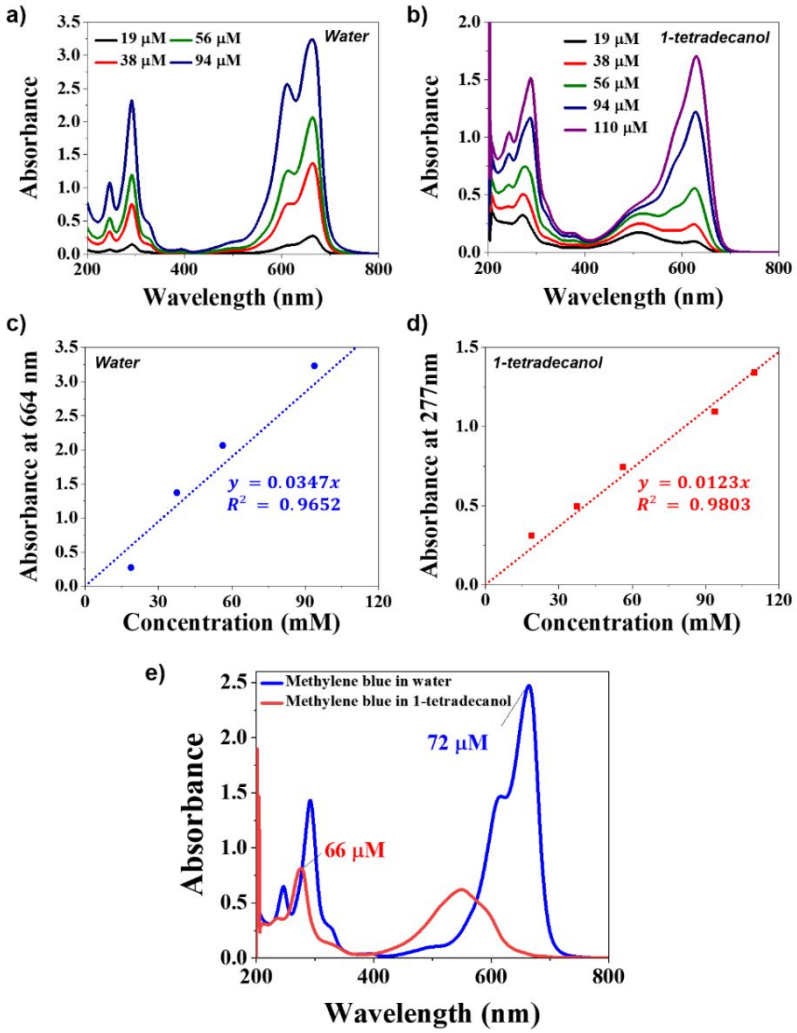

Figure S6. a, b) Ultraviolet-visible light (UV-VIS) absorbance spectra of methylene blue dissolved in water (a) and 1-tetradecanol (b) with various concentrations. c, d) Absorbance-concentration

relationships obtained from (a) and (b) for water (c) and 1-tetradecanol (d), respectively. e) Absorbance spectra of methylene blue measured from water-rich phase and 1-tetradecanol-rich phase after incubating the mixture of water and 1-tetradecanol containing methylene blue at 50°C for a day.

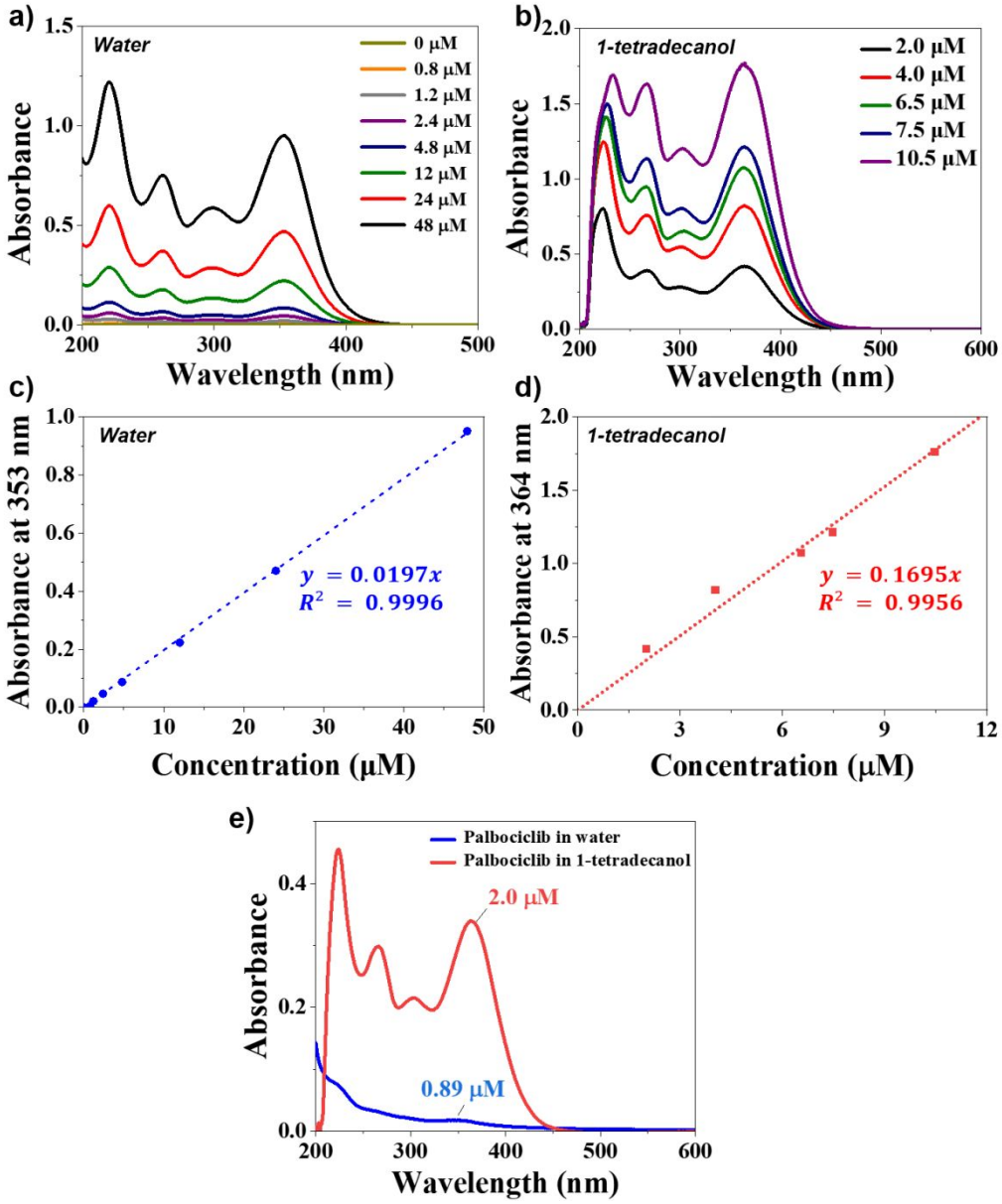

Figure S7. a, b) UV-VIS absorbance spectra of palbociclib isethionate dissolved in water (a) and 1-tetradecanol (b) with various concentrations. c, d) Absorbance-concentration relationships obtained from (a) and (b) for water (c) and 1-tetradecanol (d), respectively. e) Absorbance spectra of palbociclib isethionate measured from water-rich phase and 1-tetradecanol-rich phase after incubating the mixture of water and 1-tetradecanol containing palbociclib isethionate at 50°C for a day.

S8. Microcapsules in cuvette

Figure S8. Photograph of a quartz cuvette containing the microcapsules at the bottom.

S9. High stability of microcapsules

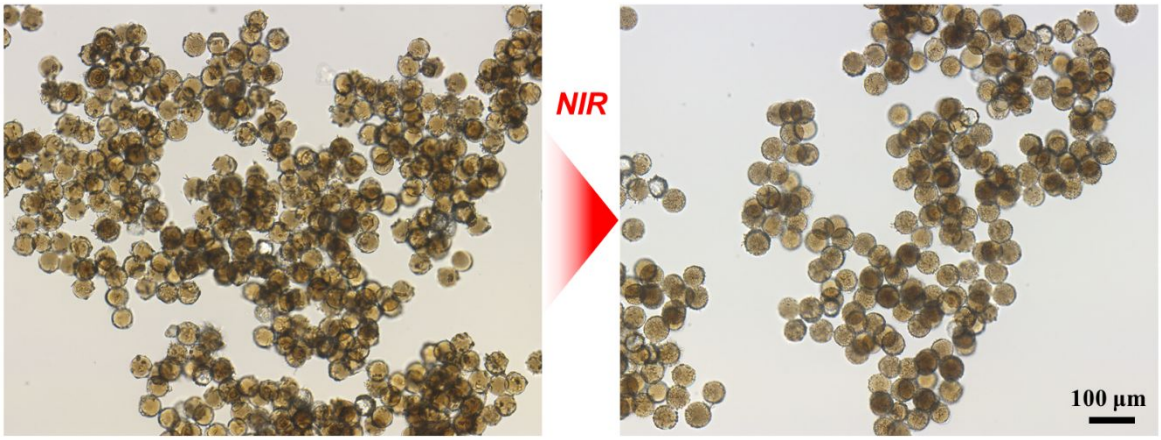

Figure S9. Transmission optical microscope images of palbociclib-isethionate-laden microcapsules before and after a photothermal heating with 808-nm-laser irradiation.

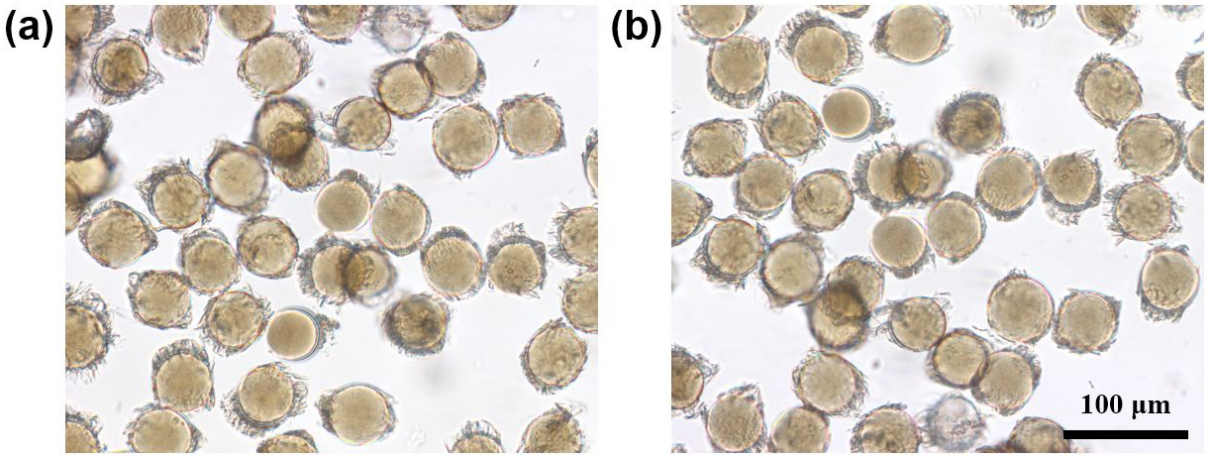

Figure S10. Transmission optical microscope images of palbociclib-isethionate-laden microcapsules after incubation at (a) 70˚C for 10 days and (b) 36.5˚C for70 days.

S10. Biocompatibility of microcapsules

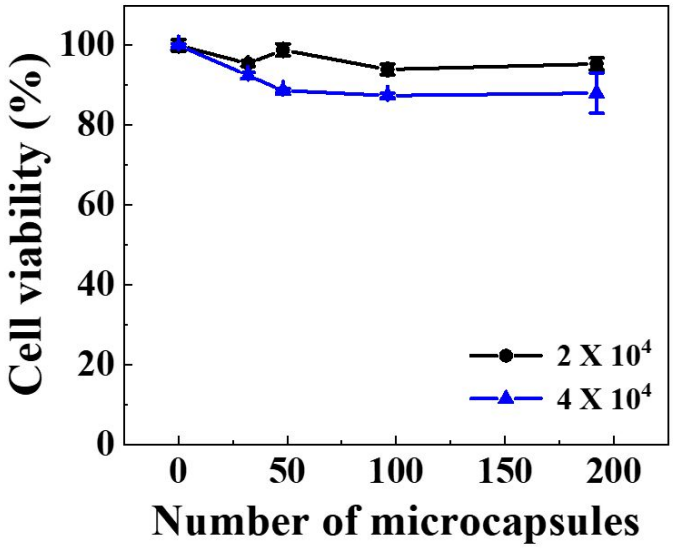

Figure S11. Cell viability test conducted by MTT assay of an epithelial human breast cancer cell line for various numbers of microcapsules after 24 h at room temperature, where two cell densities (2×10^4 and 4×10^4 cells per 100 μL) are used.

S11. Movie descriptions

Movie S1
The microfluidic production and the shrinkage of water-in-oil-in-water (W/O/W) double-emulsion droplets with an ultra-thin shell. The movie is played 10 times slower than the real time.

Movie S2
The microcapsules showing a reversible change of states depending on temperature, where the temperature is increased from 25°C to 50°C in the first half and decreased from 50°C to 25°C in the second half. The movie is played 10 times faster than the real time.

Movie S3
The temperature distribution in a chamber containing microcapsules under 808-nm-laser irradiation monitored with an infrared (IR) camera. The movie is played 30 times faster than the real time.

Movie S4
Temperature change of microcapsule-laden cuvette under 808-nm-laser irradiation for 90 s and cooling for 30 s. The movie is played 30 times faster than the real time.